Supporting Information

Guo et al. 10.1073/pnas.1410826111

SI Text

SI Methods

Materials. The surfactant n-dodecyl-β-D-maltoside (DDM) was purchased from Acros Organics. Mouse monoclonal 1D4 antibody, specific to the C terminus of rhodopsin, was purchased from the University of British Columbia, and the 1D5 peptide (TETSQVAPA, corresponding to the C-terminal epitope) was synthesized by the W. M. Keck Foundation Biotechnology Resource Laboratory at Yale University. All other chemicals were purchased from Sigma-Aldrich.

Kinetic Model. We previously reported that rhodopsin undergoes thermal decay through two pathways (Fig. S1): (*i*) the retinyl chromophore first isomerizes (k_{TI}) to form a metarhodopsin II-like product and then the protonated Schiff base (PSB) of the all-*trans* retinyl chromophore hydrolyzes ($k_{SBHMetaII}$) and (*ii*) the PSB hydrolyzes first resulting in the free 11-*cis* retinal (k_{SBH}) and then 11-*cis* retinal isomerizes in the presence of opsin (k_{ISO}). A detailed description of the kinetic model can be found in Liu et al. (1).

Kinetic Measurements. We obtained the rate constants (k_{TI}, k_{SBH}, $k_{SBHMetaII}$, and k_{ISO}) using the kinetic model (Fig. S1) by performing four experiments: (*i*) thermal decay, (*ii*) HPLC analysis, (*iii*) acid denaturation assay, and (*iv*) hydrolysis of Schiff base in metarhodopsin II (Meta II, the active state of rhodopsin), which are described in detail by Liu et al. (1).

We measured the rate of thermal decay of dark-state rhodopsin, using UV-visible spectroscopy. The visible absorption at 500 nm unique to dark-state rhodopsin was monitored. The experiment started with equilibrating buffer A in a water-jacketed cuvette at a selected temperature that was monitored during the experiment using a thermocouple. At $t = 0$, 100 μL of ice-cold concentrated rhodopsin solution was added into the preincubated buffer (3 mL) to a final concentration of 1–3 μM. The temperature change brought by the ice-cold rhodopsin sample was compensated within 5 s in control experiments. UV-visible spectra were recorded over time.

At various time points during the thermal decay experiments, 200 μL of the sample was taken out from the cuvette and placed on ice to quench thermal reactions. These samples were then split into two for the HPLC analysis and acid denaturation assay to access the extent of thermal isomerization and hydrolysis of the PSB, respectively. First, the retinyl chromophore or retinal in the samples was extracted as retinaloxime. Its isomeric composition, e.g., 11-*cis* and all-*trans*, was analyzed by HPLC to reveal the extent of thermal isomerization. Second, the samples were denatured with HCl at pH 1–2, followed by analysis using UV-visible spectroscopy. The optical density at 440 nm, a characteristic UV-visible absorption of an intact PSB, was used to quantify the extent of hydrolysis of the PSB.

To obtain the rate constants using the kinetic model, we needed to independently measure the rate of hydrolysis of Schiff base in Meta II (1). Purified rhodopsin samples were photobleached to form Meta II. At time $t = 0$, the bleached sample was added to buffer A incubated at various temperatures. Aliquots of 100 μL were removed at various time points, denatured using HCl at a final pH of 1–2, and analyzed by UV-visible spectroscopy to quantify the extent of hydrolysis of the Schiff base.

The above four experiments provided the kinetic data for global fitting to the kinetic model (1), from which we obtained the rate constants for the Arrhenius plots (Fig. S2).

Kinetic Results. We measured the rate of thermal decay by monitoring the decrease of the 500-nm absorbance at various temperatures (52.0 °C, 54.6 °C, 55.0 °C, 58.6 °C, 60.0 °C, and 64.6 °C). The data at 60.0 °C are shown in Fig. 2*A*, whereas the data for the other five temperatures are shown in Fig. S2. At time $t = 0$, a concentrated rhodopsin sample was added to preheated buffer incubated at the temperatures to ∼1 μM. A series of UV-visible spectra was collected at various time points (Fig. S2 *A–D*). Over time, OD_{500} decreases, indicating thermal decay of rhodopsin. The spectra were normalized to OD_{280} to account for solvent evaporation and then to OD_{500} at $t = 0$. At 64.6 °C, because the thermal decay process is much faster than the time needed to scan the spectrum, we fixed the wavelength of the spectrometer and directly monitored OD_{500} over time (Fig. S2*I*). The completion of the thermal decay process at 64.6 °C was confirmed by the spectrum taken after the measurement that showed the disappearance of the 500-nm peak. The normalized OD_{500} was plotted as a function of time for various temperatures (Fig. S2 *E–I*).

We also performed the other three kinetic experiments (HPLC analysis, acid denaturation assay, and hydrolysis of Schiff base in Meta II) at five temperatures and fitted the data to the kinetic model as previously described (1). From the fitting, we obtained the k_{TI} and k_{SBH} at various temperatures for the Arrhenius plots presented in Fig. S2 *E* and *F*.

Measurements of Melting Temperature. Melting temperatures of dark-state WT rhodopsin in buffer A were measured using circular dichroism (CD) spectroscopy at 1.25 μM. Molar ellipticity at 222 nm (θ_{222nm}) was monitored using a CD spectrometer (Jasco 810) while the temperature of the samples was scanned at constant rates of 60, 90, and 120 °C/h. Molar ellipticity was then fitted to a Boltzmann sigmoid equation

$$\theta_{222nm}(T) = \theta_{222nm}(base) + \frac{\theta_{222nm}(max) - \theta_{222nm}(base)}{1 + \exp\left(\frac{T_m - T}{slope}\right)}, \quad \textbf{[S1]}$$

where $\theta_{222nm}(base)$, $\theta_{222nm}(max)$, slope, and T_m are the fitting parameters. $\theta_{222nm}(base)$ and $\theta_{222nm}(max)$ are the values of minimum and maximum intensities, respectively. The reported melting temperature, T_m, is the inflection point of the sigmoidal curve. The slope describes how fast the signal increases around the melting temperature. Table S1 summarizes the results of the fitting.

Analysis of Melting Curve. We analyzed the melting curve using the Van't Hoff equation to obtain ΔH_m and ΔS_m for the melting process, assuming that the melting of rhodopsin is a two-state process

$$folded \rightleftharpoons unfolded. \quad \textbf{[S2]}$$

The equilibrium constant for the unfolding process is

$$K_{eq} = \frac{f_{unfolded}}{f_{folded}} = \exp\left(-\frac{\Delta G_m}{RT}\right), \quad \textbf{[S3]}$$

where $f_{unfolded}$ and f_{folded} are the fractions of protein in the unfolded and folded states, respectively. They can be expressed as

$$f_{unfolded} = \frac{\theta_{222nm}(T) - \theta_{222nm}(base)}{\theta_{222nm}(max) - \theta_{222nm}(base)}, \quad [S4]$$

$$f_{folded} = \frac{\theta_{222nm}(max) - \theta_{222nm}(T)}{\theta_{222nm}(max) - \theta_{222nm}(base)}, \quad [S5]$$

where $\theta_{222nm}(T)$, $\theta_{222nm}(base)$, and $\theta_{222nm}(max)$ are the intensities at temperature (T) and the minimum and maximum intensities, respectively.

Substituting Eqs. **S4** and **S5** into Eq. **S3** yields

$$K_{eq} = \frac{\theta_{222nm}(T) - \theta_{222nm}(base)}{\theta_{222nm}(max) - \theta_{222nm}(T)} = \exp\left(-\frac{\Delta H_m - T\Delta S_m}{RT}\right). \quad [S6]$$

Hence, $\theta_{222nm}(T)$ can be expressed as

$$\theta_{222nm}(T) = \frac{\theta_{222nm}(base) + \theta_{222nm}(max) \times \exp\left(-\frac{\Delta H_m - T\Delta S_m}{RT}\right)}{\exp\left(-\frac{\Delta H_m - T\Delta S_m}{RT}\right) + 1}. \quad [S7]$$

Thus, Eq. **S7** can be used to analyze the melting curve to obtain the fitting parameters of $\theta_{222nm}(base)$, $\theta_{222nm}(max)$, ΔH_m, and ΔS_m. The fitted values of ΔH_m and ΔS_m are summarized in Table S2.

Transition State Theory

The starting point for our analysis is the standard transition state theory (TST) expression for the unimolecular reaction rate constant k given by Eq. **1**. Although Eq. **1** is a familiar one, it is useful to state the assumptions on which it is based. For a system with N coordinates, the transition state is defined to be an $N - 1$ dimensional hypersurface that completely separates the reactant region of configuration space from the product region; i.e., any trajectory in configuration space that evolves from reactants to products must pass through the dividing surface at least once. Thus, the transition state is not just a local region near a saddle point on the potential energy surface, it is an extended, $N - 1$ dimensional hypersurface. Eq. **1** is simply the classical mechanical equilibrium one-way flux through the dividing surface in the direction of reactants to products, and can be derived under three approximations. First, classical mechanics is valid; i.e., quantum effects on nuclear motion can be neglected. Second, recrossing corrections—the overestimate of the reaction rate because some trajectories may cross the dividing plane more than once in evolving from reactants to products—are unimportant. Third, one reaction coordinate degree of freedom of the reactant can be singled out as a separable harmonic high-frequency vibration of frequency w, $\hbar\omega \gg k_B T$. Note that if w is in the low-frequency limit, $\hbar\omega \ll k_B T$, the factor $k_B T/h$ is replaced by $\omega/2\pi$ in Eq. **1**. In either case this factor is of order 10^{13} s^{-1}, and the weak temperature dependence in the first form is negligible for the current arguments. These three approximations need to be examined when computing rate constants to quantitative accuracy, but it is unlikely they have any significant effect on the qualitative picture presented here.

Within the assumptions of transition state theory and from Eq. **1**, we obtain

$$\ln k = \ln T + \ln\frac{k_B}{h} + \frac{\Delta S^{\ddagger}}{k_B} - \frac{\Delta H^{\ddagger}}{k_B T}. \quad [S8]$$

The partial derivative of ln$k$ with respect to T gives

$$\frac{\partial \ln k}{\partial T} = \frac{1}{T} + \frac{\Delta H^{\ddagger}}{k_B T^2}. \quad [S9]$$

In the Arrhenius plot, the activation energy E_a is defined as

$$E_a = -k_B \frac{\partial \ln k}{\partial (1/T)}\bigg|_{T=T_0} = k_B T_0^2 \frac{\partial \ln k}{\partial T}\bigg|_{T=T_0}. \quad [S10]$$

Subsituting Eq. **S9** into Eq. **S10** gives Eq. **2**.

In the Arrhenius plot, the preexponential factor A_{pref} is defined as follows:

$$A_{pref} = k(\beta_0)\exp\left(-\beta_0 \frac{\partial \ln k}{\partial \beta}\bigg|_{\beta=\beta_0}\right), \quad [S11]$$
$$= \frac{k_B T_0}{h} e^{\frac{\Delta S_0^{\ddagger}}{k_B}} e^{-\frac{\Delta H_0^{\ddagger}}{k_B T_0}} e^{\beta_0 Ea}.$$

Keeping the entropic term on the left side

$$e^{\frac{\Delta S_0^{\ddagger}}{k_B}} = \frac{A_{pref} h}{k_B T_0} e^{\frac{\Delta H_0^{\ddagger}}{k_B}} e^{-\frac{E_a}{k_B T}}. \quad [S12]$$

Taking the log on both sides

$$\frac{\Delta S_0^{\ddagger}}{k_B} = \ln\left(A_{pref} h / k_B T_0\right) + \frac{\Delta H_0^{\ddagger}}{k_B} - \frac{E_a}{k_B T}. \quad [S13]$$

Substituting Eq. **2** into Eq. **S13** gives Eq. **3**.

Quantum Mechanics/Molecular Mechanics Methodology

System Setup. We started from the X-ray structure available for bovine rhodopsin [Protein Data Bank (PDB) code: 1U19; resolution, 2.2 Å] (2), which has no missing amino acids. We included only the protein chain A and the corresponding water chain of the crystallographic dimer. In total, 37 water molecules are added to the system. Non-amino acid residues at the protein surface (membrane lipids), as well as Hg and Zn ions, were omitted. A water molecule was put in the place of surface ion Zn963 for matching its interaction with His278. Met1 was acetylated as in the X-ray structure, and the C terminus was used for Ala348. The results of PROPKA (3) and PROCHECK (4, 5) programs were used, in combination with visual inspection, to assign the protonation states of all titratable residues. Asp83, Glu122, Glu181, and Glu249 were protonated (neutralized). Previous experimental (6, 7) and computational studies (8, 9) of site-directed mutants indicate that these residues are neutral. Thus, in the active site, for E181, charges of the carboxylate oxygens and hydrogen were zeroed, whereas for E113, only one of the carboxylate oxygens (OE1) was zeroed so that the other (OE2) was allowed to stabilize the positively charged PSB. Residues His152 and His211 are protonated at the ε nitrogen and His195 and His278 are protonated at the δ nitrogen. The other histidines (His65 and His100) are protonated at both nitrogen atoms. Residues Cys110 and Cys187 form a disulfide bond, and standard protonation states are used for all other amino acid residues. The overall charge of the system after adding the missing hydrogen atoms (total of 5,632 atoms) is +1*e*.

Molecular Mechanics Calculations. All molecular mechanics (MM) calculations, pure MM or hybrid ONIOM (our own n-layered integrated molecular orbital and molecular mechanics) [quantum mechanics (QM)/MM), were performed with the assisted model building with energy refinement (AMBER) all-atom force field and three-site transferable intermolecular potential water model (10). All available force field parameters and charges and types

of each atom in each amino acid were taken from the AMBER library (10). The entire rhodopsin system was first optimized at a pure AMBER force field level to remove close contacts. The resulting geometries were used as the initial geometries of ONIOM optimizations. During the pure AMBER and the ONIOM geometry optimizations, no restraints were applied. The positions of backbone atoms in the seven transmembrane α-helices of rhodopsin were well conserved during optimization.

ONIOM Hybrid Calculations. QM/MM calculations were performed with the use of the ONIOM method. In this case, we used the two-layer ONIOM (QM:MM) scheme (11–13), in which the interface between QM (the PSB of 11-*cis* retinyl chromophore) and MM (opsin) region is treated by hydrogen link atom (14). To be specific, the total energy of the system (E^{ONIOM}) is obtained from three independent calculations

$$E^{\mathrm{ONIOM}} = E^{\mathrm{MM}}_{\mathbf{1+2}} - E^{\mathrm{MM}}_{\mathbf{2}} + E^{\mathrm{QM}}_{\mathbf{2}},$$

where $E^{\mathrm{MM}}_{\mathbf{1+2}}$ is the MM energy of the entire system (including both retinyl chromophore and opsin), called the real system in ONIOM terminology; $E^{\mathrm{MM}}_{\mathbf{2}}$ is the MM energy of a part of the real system that has main chemical interest (retinyl chromophore), called the model part (Fig. S3); and $E^{\mathrm{QM}}_{\mathbf{2}}$ is the QM energy of the retinyl chromophore.

In this study, electrostatic interactions between the two layers were calculated using the electronic embedding (EE) scheme. In the EE scheme, the electrostatic interactions between the two layers are present in all three energy terms. Thus, the electrostatic interaction terms included at the MM energies ($E^{\mathrm{MM}}_{\mathbf{1+2}}$ and $E^{\mathrm{MM}}_{\mathbf{2}}$) cancel out, leaving only the interaction energy term that also includes polarization of the wave function of the model part (retinyl chromophore) by the surrounding point charges of the opsin ($E^{\mathrm{QM}}_{\mathbf{2}}$). Therefore, according to this QM/MM methodology, the energy of protein **1**, described at the MM level, with an embedded chromophore **2,** described according to QM density functional theory, is obtained as the MM energy of the complete system $E^{\mathrm{MM}}_{\mathbf{1+2}}$ minus the MM energy of chromophore $E^{\mathrm{MM}}_{\mathbf{2}}$ interacting with the environment. Relaxed intermediate structures, along the resulting isomerization minimum energy path, are obtained subject to constraint of incremental changes of the dihedral angle ($\varphi_{C11=C12}$) in the −17° (*cis*) to −180° (*trans*) range, relaxing the configuration of residues and waters within a 4.0-Å radius from any atom of the retinyl chromophore. The TS configuration is found at $\varphi_{C11=C12} = -116°$. Configurations with disrupted H-bonds are obtained by optimizing the geometry of the system after zeroing the atomic charges of selected water molecules and H-bonding partners.

Tracing the Transition State. We obtained the geometry of the transition state of the retinyl chromophore by generating the relaxed intermediate structures of the retinyl chromophore along the ground-state minimum energy path (S_0-MEP), subject to the constraints of a fixed dihedral angle about the isomerizing C11-C12 double bond. Geometry optimization was performed at the ONIOM-EE (B3LYP/6–31G*:Amber96) (10, 15–17) level of theory implemented in the Gaussian09 module (4) by incrementally rotating the dihedral angle, $\varphi_{C11=C12}$, to −120° in the presence of a relaxed protein environment, where the following residues within the 4.0-Å radius to any atom of the retinyl chromophore were relaxed: Tyr43, Met44, Leu47, Met86, Phe91, Thr94, Glu113, Gly114, Ala117, Thr118, Gly121, Glu122, Leu125, Tyr178, Glu181, Ser186, Cys187, Gly188, Ile189, Tyr191, Met207, Phe208, His211, Phe212, Phe261, Trp265, Tyr268, Ala269, Ala292, Phe293, Phe294, Ala295, Lys296, Thr297, Ser298, Ala299, w1, and w2. The resulting structure was then relaxed without any further constraints in the dihedral angle.

QM/MM-EE Minimum Energy Path Computation of the Transition State During the Isomerization Event in Bovine Rhodopsin. We calculated the total energy of the system by incrementally rotating the C11-C12 dihedral angle, $\varphi_{C11=C12}$, from −17° to −120°. Because it is computationally expensive to perform frequency calculations for the full protein at the QM/MM-EE scheme, the transition state determined is not a true first-order saddle point in multidimensional space. We determined the saddle point energy between *cis* and *trans* states, i.e., the minimum energy at the transition state by an increment of about 20° from −17° to −80°, and a 5° increment from −80° to −120°. As shown in Table S3, the total energy of the system increases when $\varphi_{C11=C12}$ changes from −17° to −116° and then starts to decrease from −116° to −120°. At this point, we performed further incremental rotation of the $\varphi_{C11=C12}$ by 1° until we reached the saddle point at −116° (labeled in bold). This structure is referred as TS and used for the ensuing QM/MM calculations.

QM/MM Energy Decomposition Analysis of the Isomerization Reaction Barrier. After determining the transition state, the following scheme (Fig. S3) was used to perform the energy decomposition analysis of the isomerization reaction barrier of retinyl chromophore in rhodopsin:

$$\Delta E_{Total} = \Delta E^{\mathrm{ONIOM}} = \Delta E_{Retinal} + \Delta E_{Protein},$$

$$\Delta E_{Protein} = \Delta E^{\mathrm{MM,Real}} - \Delta E^{\mathrm{MM,Model}},$$

$$\Delta E_{Retinal} = \Delta E^{\mathrm{QM,Model}}.$$

We did the calculation for the reaction barrier of isomerization ($\Delta E_{Retinal}$) in two cases: (*i*) all of the H-bonds in the EII loop are broken and (*ii*) all of the H-bonds in the EII loop and all of the water molecules are randomized. In both cases, the reaction barrier (labeled in red in Table S4) of isomerization decreases from 40 to ∼28 kcal/mol.

Estimation of $\Delta G^{\ddagger}$ from the QM/MM Results

At low temperatures with $\Delta H^{\ddagger}_2 = 40$ kcal/mol at $T_0 = 40$ °C, $\Delta G^{\ddagger} \approx \Delta G^{\ddagger}_2 = \Delta H^{\ddagger}_2 - T_0 \Delta S^{\ddagger}_2$ is ∼39 kcal/mol. At intermediate temperatures where the enthalpic ($\Delta H^{\ddagger}_1$) and entropic terms ($T\Delta S^{\ddagger}_1$) offset each other (i.e., $\Delta G^{\ddagger}_1 = \Delta H^{\ddagger}_1 - T\Delta S^{\ddagger}_1 \rightarrow 0$), the activation barrier $\Delta G^{\ddagger}$ is roughly equal to $\Delta G^{\ddagger}_2$ ∼27 kcal/mol ($\Delta H^{\ddagger}_2 = 28$ kcal/mol and $T_0 = 55$ °C). At high temperatures, the computed reaction barrier, $\Delta G^{\ddagger} \approx \Delta G^{\ddagger}_2$, is ∼26 kcal/mol using $\Delta H^{\ddagger}_2 = 28$ kcal/mol at $T_0 = 75$ °C.

1. Liu J, Liu MY, Fu L, Zhu GA, Yan EC (2011) Chemical kinetic analysis of thermal decay of rhodopsin reveals unusual energetics of thermal isomerization and hydrolysis of Schiff base. *J Biol Chem* 286(44):38408–38416.
2. Okada T, et al. (2004) The retinal conformation and its environment in rhodopsin in light of a new 2.2 A crystal structure. *J Mol Biol* 342(2):571–583.
3. Li H, Robertson AD, Jensen JH (2005) Very fast empirical prediction and rationalization of protein pKa values. *Proteins* 61(4):704–721.
4. Laskowski RA, Macarthur MW, Moss DS, Thornton JM (1993) Procheck: A program to check the stereochemical quality of protein structures. *J Appl Cryst* 26(2):283–291.
5. Morris AL, MacArthur MW, Hutchinson EG, Thornton JM (1992) Stereochemical quality of protein structure coordinates. *Proteins* 12(4):345–364.
6. Sakmar TP, Franke RR, Khorana HG (1989) Glutamic acid-113 serves as the retinylidene Schiff base counterion in bovine rhodopsin. *Proc Natl Acad Sci USA* 86(21):8309–8313.
7. Zhukovsky EA, Oprian DD (1989) Effect of carboxylic acid side chains on the absorption maximum of visual pigments. *Science* 246(4932):928–930.
8. Sekharan S, Buss V (2008) Glutamic acid 181 is uncharged in dark-adapted visual rhodopsin. *J Am Chem Soc* 130(51):17220–17221.
9. Altun A, Yokoyama S, Morokuma K (2008) Spectral tuning in visual pigments: an ONIOM(QM:MM) study on bovine rhodopsin and its mutants. *J Phys Chem B* 112(22): 6814–6827.
10. Cornell WD, et al. (1995) A 2nd generation force-field for the simulation of proteins, nucleic acids, and organic molecules. *J Am Chem Soc* 117(19):5179–5197.

11. Maseras F, Morokuma K (1995) Imomm: A new integrated ab-initio plus molecular mechanics geometry optimization scheme of equilibrium structures and transition states. *J Comput Chem* 16(9):1170–1179.
12. Dapprich S, et al. (1999) A new ONIOM implementation in Gaussian98. Part I. The calculation of energies, gradients, vibrational frequencies and electric field derivatives. *J Mol Struc-Theochem* 461:1–21.
13. Vreven T, et al. (2006) Combining quantum mechanics methods with molecular mechanics methods in ONIOM. *J Chem Theory Comput* 2(3):815–826.
14. Bakowies D, Thiel W (1996) Hybrid models for combined quantum mechanical and molecular mechanical approaches. *J Phys Chem-Us* 100(25):10580–10594.
15. Becke AD (1988) Density-functional exchange-energy approximation with correct asymptotic behavior. *Phys Rev A* 38(6):3098–3100.
16. Lee C, Yang W, Parr RG (1988) Development of the Colle-Salvetti correlation-energy formula into a functional of the electron density. *Phys Rev B Condens Matter* 37(2):785–789.
17. Becke AD (1993) Density-functional thermochemistry. III. The role of exact exchange. *J Chem Phys* 98(7):5648–5652.

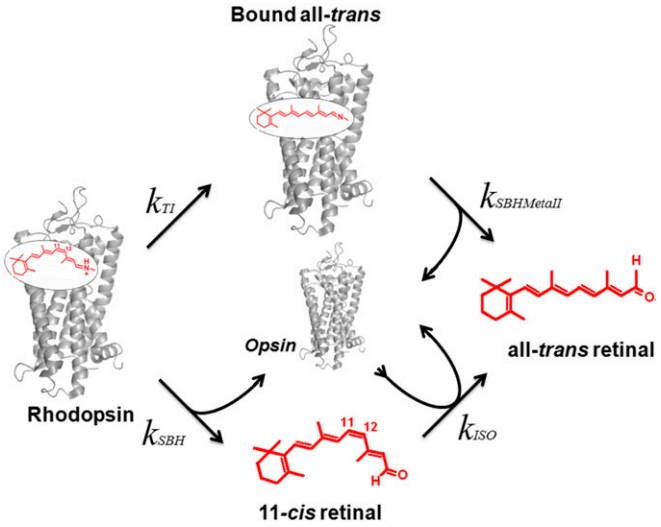

Fig. S1. Kinetic model of the thermal processes in rhodopsin.

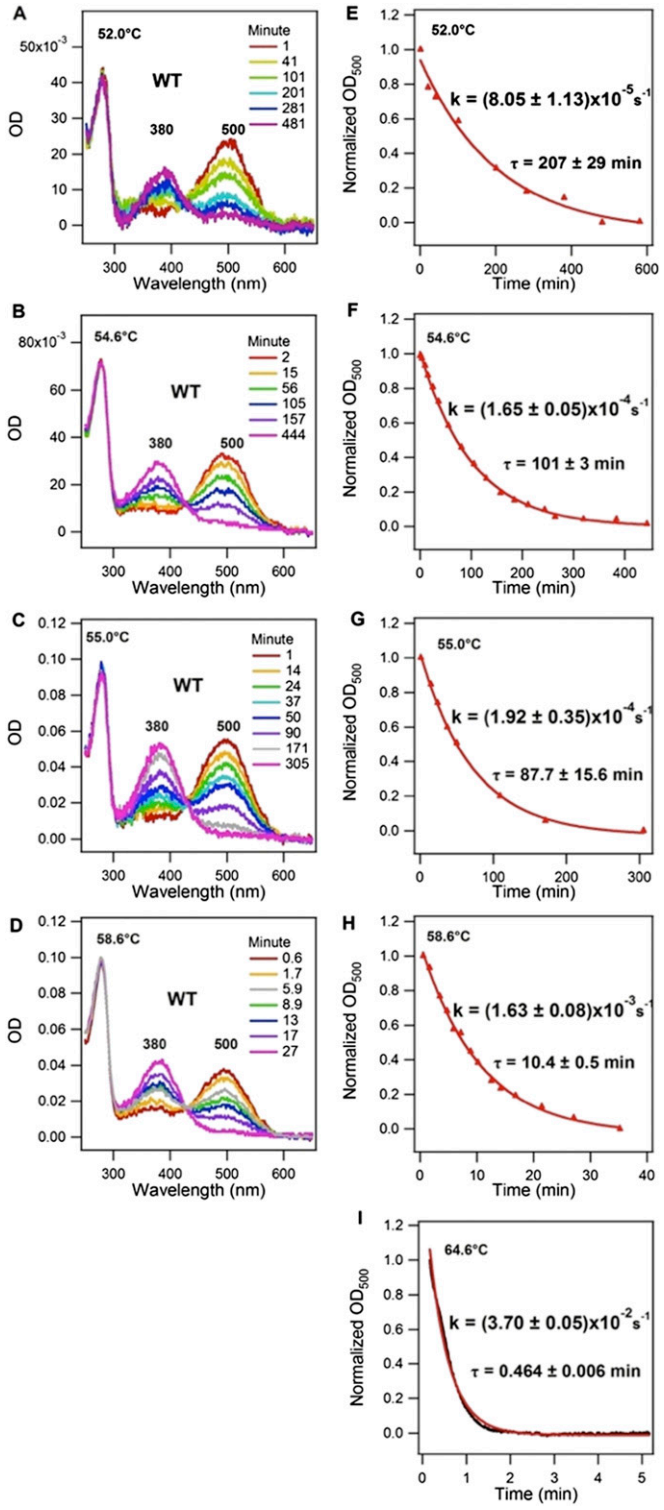

Fig. S2. Kinetics of thermal decay of WT rhodopsin at various temperatures. UV-visible spectra of WT rhodopsin obtained at (*A*) 52.0 °C, (*B*) 54.6 °C, (*C*) 55.0 °C, and (*D*) 58.6 °C. Over time, OD_{500} decreases, whereas OD_{380} increases. Normalized OD_{500} plotted as a function of time for (*E*) 52.0 °C, (*F*) 54.6 °C, (*G*) 55.0 °C, (*H*) 58.6 °C, and (*I*) 64.6 °C, which is fitted to a single exponential function (—) to determine the decay time and rate constant.

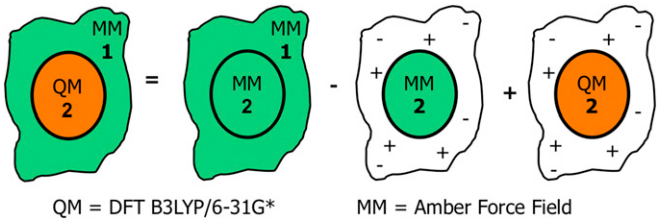

Fig. S3. Schematic representation of the two-layer ONIOM (QM:MM) scheme adopted in this study, where the ONIOM energy is $E^{\mathrm{ONIOM}} = E^{\mathrm{MM}}_{1+2} - E^{\mathrm{MM}}_{2} + E^{\mathrm{QM}}_{2}$.

Table S1. Melting temperatures and fitting parameters for WT rhodopsin

Scanning rate	120 °C/h	90 °C/h		60 °C/h	
T_m (°C)	69.0 ± 0.3	70.8 ± 0.4	69.9 ± 0.3	68.6 ± 0.3	69.3 ± 0.2
θ_{222nm}(base)	−72.4 ± 0.4	34.5 ± 0.2	−27.8 ± 0.2	−27.4 ± 0.2	−50.4 ± 0.1
θ_{222nm}(max)	−42.0 ± 0.4	−25.3 ± 0.6	−16.1 ± 0.5	18.5 ± 0.4	−35.8 ± 0.6
Slope	1.82 ± 0.27	1.02 ± 0.32	1.13 ± 0.26	0.88 ± 0.28	1.32 ± 0.16

Table S2. Enthalpy and entropy changes for the melting process of WT rhodopsin

Scanning rate	120 °C/h		90 °C/h		60 °C/h	
ΔH_m (kcal/mol)	149 ± 13	221 ± 31	170 ± 19	170 ± 35	197 ± 26	165 ± 16
ΔS_m (kcal/molK)	0.437 ± 0.038	0.644 ± 0.089	0.495 ± 0.055	0.497 ± 0.101	0.579 ± 0.077	0.482 ± 0.048

Table S3. Tracing the transition state during the *cis*-to-*trans* isomerization of bovine rhodopsin

$\varphi_{C11=C12}$, (°)	*cis*-to-*trans* isomerization of bovine rhodopsin
−17°	−850.837418 (0.000)
−40°	−850.834411 (1.887)
−60°	−850.825445 (7.513)
−80°	−850.810946 (16.611)
−85°	−850.806555 (19.367)
−90°	−850.801901 (22.287)
−95°	−850.797059 (25.327)
−100°	−850.792065 (28.459)
−105°	−850.786995 (31.641)
−110°	−850.782352 (34.554)
−115°	−850.777801 (37.410)
−116°	**−850.776969 (37.932)**
−117°	−850.802297 (22.039)
−118°	−850.802598 (21.850)
−119°	−850.802885 (19.783)
−120°	−850.803158 (21.498)

Residues within 4.0-Å radius to any atom of the retinyl chromophore are relaxed during the calculation. Absolute energies are given in Hartrees, and relative energies are given in kcal/mol in parentheses. The saddle point values are indicated in bold.

Table S4. Energy decomposition analysis of the isomerization reaction barrier in bovine rhodopsin

Bovine rhodopsin models (°C)	$E^{MM}{}_2$	$E^{MM}{}_{2+1}$	$E^{QM}{}_2$
WT (−17°)	−0.030196 (34.960)	−16.022583 (32.347)	−834.845031 (40.546)
TS (−116°)	0.025516 (0.000)	−15.971035 (0.000)	−834.780417 (0.000)
Barrier: (32.347 − 34.960) + 40.546 = 37.933 kcal/mol			
Case 1: H-bonds in the EII loop are broken			
WT (−17°)	−0.030196 (23.032)	−16.022583 (101.595)	−834.845031 (27.555)
TS (−116°)	0.006508 (0.000)	−15.860681 (0.000)	−834.801120 (0.000)
Barrier: (101.595 − 23.032) + 27.555 = 106.118 kcal/mol			
Case 2: H-bonds associated with the EII loop and internal water molecules are randomized			
WT (−17°)	−0.030196 (24.254)	−16.022583 (533.355)	−834.845031 (27.610)
TS (−116°)	0.008456 (0.000)	−15.172629 (0.000)	−834.801031 (0.000)
Barrier: (533.355 − 24.254) + 27.610 = 536.711 kcal/mol			